COVER PAGE

Bibliographical reference

Calculation of Reflections in an Urban Environment, Kurt Heutschi, Acta Acustica **vol. 95** (Number 4), 2009, pp. 644-652

DOI

https://doi.org/10.3813/AAA.918193

ACTA ACUSTICA UNITED WITH ACUSTICA
Vol. 95 (2009) 644 – 652

DOI 10.3813/AAA.918193

Calculation of Reflections in an Urban Environment

Kurt Heutschi
Empa, Swiss Federal Laboratories for Materials Testing and Research, 8600 Duebendorf, Switzerland.
Kurt.Heutschi@emps.ch

Summary
Sound propagation in an urban environment is often significantly influenced by reflections at building façades. The façades are typically structured in depth in the order of magnitude of decimeters up to meters. Low frequency reflections tend thus to be mirror like while at high frequencies they get a more and more diffuse or scattering character. A model is presented to calculate the effects of both type of reflections. After a discretization of the boundaries into grid cells, the sound pressure and energy exchange between the patches is calculated step by step. A coherent model is established to handle specular reflections. It solves a Kirchhoff-Helmholtz formulation by a time iterative process. The incoherent model for diffuse reflections assumes energy conservation and Lambert distribution for the reflections. The advantage of the model - which is part of the new Swiss railway noise calculation scheme sonRAIL - is its continuous behavior and the ability to take into account the reflector size. The model for specular reflections was validated extensively and proofed to reproduce scale model experiments as well as numerical FDTD simulations with good accuracy.

PACS no. 43.28.En, 43.28.Js, 43.50.Rq

1. Introduction

In contrast to a free field situation, sound propagation in an urban environment is strongly influenced by reflections and possible shielding effects. For extended or moving sources like roads or railway lines, diffraction can often be neglected as the total received sound energy is dominated by the contribution of direct and reflected sound. Reflections do occur at building façades which are usually acoustically hard with no or little absorption. Typically such façades show more or less pronounced structures with a depth stepping in the order of decimeters up to meters. Depending on the frequency of interest, the resulting sound reflection is thus more likely specular or diffuse.

The influence of reflections on sound immission can be determined in principle by scale model experiments [1, 2]. However, investigations with many receiver positions make calculation procedures necessary. An excellent overview of the state of knowledge can be found in [3, 4] and in the book by Kang [5].

A first category of calculation schemes are empirical models that predict the influence of buildings in an integral way [6, 7]. These models are based on few situation parameters such as building density and propagation distance. Obviously they are quite coarse and unable to model specific local geometries.

Received 4 November 2008,
accepted 8 March 2009.

The second category of models simulates sound propagation explicitly. Depending on the type of reflections, different strategies can be applied. The underlying concepts stem often from room acoustics where similar problems of multiple reflections occur. If the reflecting surfaces are assumed to be flat, homogeneous and large, the mirror source concept may be applied [8]. If the path length differences between different reflection contributions are not too small, an energetic superposition is appropriate. However, in special cases of very narrow canyons, a phase sensitive calculation may be necessary to account for interference effects [9]. In case of structured façades, at least for high frequencies, the reflections tend to become diffuse like. For the special geometry of a street canyon of given width and height, an analytical solution can be found for the diffuse field under the assumption of a uniform scattering in all directions [10]. With ray tracing algorithms diffuse reflections can be modeled for any reflection directivity, as e.g. the Lambert $\cos(\phi)$ angle dependency. Other approaches to handle diffuse reflections are the diffusion equation and the radiosity method. For special geometries the diffusion equation can be solved analytically [11]. In the general case a numerical scheme has to be applied to solve the differential equation, as e.g. the finite difference time domain method [12]. The radiosity method [13] divides the boundaries into a number of patches and simulates the energy exchange between them. The crucial point is the determination of the form factors. For each sender patch they describe the amount of energy that is transmitted to the receiver patches. The application of wave the-

oretical models [14, 15, 16] is very much limited as the large geometries demand for an extremely high computational effort.

In the following a new model is proposed with algorithms that are positioned somewhere between geometrical and wave theoretical approaches. Specular and diffuse reflections are handled separately to account for their individual behavior. The model was developed as part of the new Swiss railway noise model sonRAIL. The region of application however is not restricted to train noise. Under certain assumptions that will be discussed below, the model can be used for any source type that can be described as a combination of single point sources.

2. General considerations for a calculation model

While diffuse reflections are relatively convenient to implement, specular reflections need a more costly calculation. The difficulty with specular reflections is that they have a *memory*, which means that the exact geometry of the complete path from the source to the actual reflector is relevant. The history of a sound path is stored as phase and amplitude information of the pressure and velocity distributions on the reflecting surfaces.

Within the concept of mirror sources such a path can be determined by a billiard construction. The check of "visibility" decides whether a reflection occurs or not. However this approach usually ignores two important aspects:

- Specular reflections need a certain area on a reflecting surface. For low frequencies this area, which can be estimated by a Fresnel zone consideration, may easily become larger than the reflector itself, resulting in a corresponding attenuation.
- Specular reflections occur in real life (with an according attenuation) even if the point of reflection is not on the reflecting surface itself.

The above mentioned properties are a consequence of the wave nature of sound and the relative large wave lengths compared to typical geometrical dimensions of built structures. These aspects can be handled properly only if a calculation model is based on a wave theoretical formulation. This request usually demands for frequency domain methods such as FE (Finite Elements) or BE (Boundary Elements) or time domain methods such as FDTD (Finite Difference Time Domain).

In the present context it is assumed that diffracted sound can be ignored and thus the sound field is dominated by possible direct sound and reflections. For further calculations it is beneficial to use a priori knowledge about the development of the sound field. The essential idea is to solve a boundary element formulation in a time iterative way. This fundamental concept can be used for both specular and diffuse reflections. In any case a discretization of the reflecting surfaces into subareas is needed. The effect of the total reflection at an observer point is then calculated by a summation of the contributions of each subarea (Figure 1).

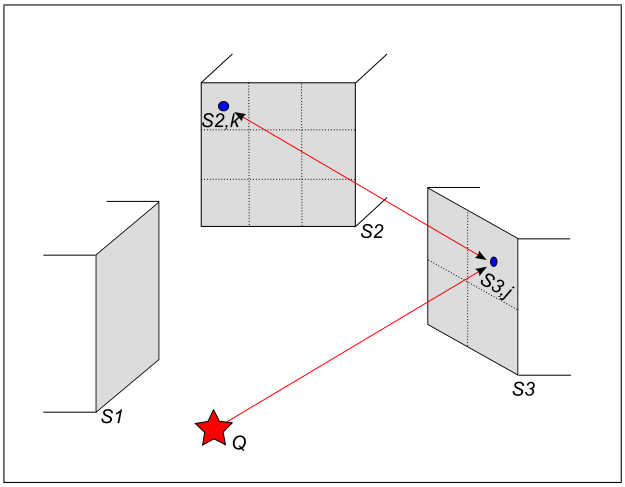

Figure 1. Concept for the calculation of reflections. The geometry shows the source Q and three reflecting surfaces S_1, S_2, S_3. Each surface S_i is divided into a suitable number of subareas or grid cells with a representative point in the middle.

For the model presented here, we assume that there is no frequency dependent ground effect and that sound pressure and energy exchange occurs only between points with direct sightline. The effect of the ground is accounted for by limiting sound source radiation to the half space only (solid angle 2π steradians). As already mentioned, specular-like and diffuse reflections have to be handled separately. Consequently, a calculation scheme for coherent reflections and one for incoherent reflections is developed.

3. Model for coherent reflections

3.1. Theoretical considerations

The coherent model is based on the Kirchhoff-Helmholtz integral

$$\check{p}(x,y,z,\omega) = \frac{1}{4\pi}\int_S \left(\mathrm{j}\omega\rho_0\check{v}_S(\omega)\frac{\mathrm{e}^{-\mathrm{j}\omega r/c}}{r} + \check{p}_S(\omega)\frac{\partial}{\partial n}\frac{\mathrm{e}^{-\mathrm{j}\omega r/c}}{r}\right)\mathrm{d}S. \quad (1)$$

Equation (1) states that the sound pressure $\check{p}(\omega)$ at any point $< x, y, z >$ in space can be expressed as a surface integral of sound velocity $\check{v}_S(\omega)$ and sound pressure $\check{p}_S(\omega)$ over a closed surface S. ω is the angular frequency, r is the distance from $< x, y, z >$ to the surface point under consideration, ρ_0 is the density and c the speed of sound. Introducing the wave number k, where

$$k = \frac{2\pi}{\lambda} = \frac{\omega}{c} \quad \Rightarrow \quad \mathrm{e}^{-\mathrm{j}\omega r/c} = \mathrm{e}^{-\mathrm{j}kr} \quad (2)$$

and evaluating the partial differentiation of the pressure contribution

$$\frac{\partial}{\partial n}\left(\frac{\mathrm{e}^{-\mathrm{j}kr}}{r}\right) = \frac{1}{r^2}\left(r\frac{\partial}{\partial n}\left(\mathrm{e}^{-\mathrm{j}kr}\right) - \mathrm{e}^{-\mathrm{j}kr}\frac{\partial r}{\partial n}\right) = \frac{1}{r^2}\left(-\mathrm{j}kr\frac{\partial r}{\partial n}\mathrm{e}^{-\mathrm{j}kr} - \mathrm{e}^{-\mathrm{j}kr}\frac{\partial r}{\partial n}\right) = \frac{1}{r^2}\mathrm{e}^{-jkr}(-jkr-1)\frac{\partial r}{\partial n}, \quad (3)$$

with

$$\frac{\partial r}{\partial n} = \cos(\phi) \quad (4)$$

and ϕ: angle between the normal direction of the surface and the direction to the point $< x, y, z >$, the Kirchhoff-Helmholtz integral can be rewritten in the following form:

$$\check{p}(x, y, z, \omega) = \frac{1}{4\pi}\int_S \left(\mathrm{j}\omega\rho_0\check{v}_S(\omega)\frac{\mathrm{e}^{-\mathrm{j}kr}}{r} + \check{p}_S(\omega)\frac{1+\mathrm{j}kr}{r^2}\cos\phi\mathrm{e}^{-\mathrm{j}kr}\right)\mathrm{d}S. \quad (5)$$

Equation (5) is solved here iteratively. For now it is assumed that the surfaces are acoustically hard which means the surface velocity $\check{v}_S$ is identical to 0.

3.2. Formulation of the algorithm

Step 1:
According to Figure 1 the façade areas S_i are divided into subareas $S_{i,j}$ of size ΔS. Initial sound pressure is set to 0 for all surface points,

$$\check{p}_{0,i,j} = 0. \quad (6)$$

Step 2:
A first estimate for the pressure distribution $\check{p}_{1,i,j}$ on the surfaces S_i is found by calculating the direct sound contribution from the source,

$$\check{p}_{1,i,j} = 2\mathrm{j}\sqrt{\frac{W\rho c}{4\pi r^2}}\mathrm{e}^{-\mathrm{j}kr}, \qquad \psi \le \frac{\pi}{2}, \quad (7)$$

where W is the sound power of the point source and ψ is the angle between the direction from the surface point to the source and the surface normal vector. The factor 2 counts for the pressure doubling on hard surfaces.
Step 3:
The n-th estimate of pressure $\check{p}_{n,i,j}$ at point j on surface S_i is found by adding the contributions of the last changes of the pressure values on all other surfaces (Figure 2).

$$\check{p}_{n,i,j} = \check{p}_{n-1,i,j} + 2\frac{1}{4\pi}\sum_s\sum_t\left(\check{p}_{n-1,s,t} - \check{p}_{n-2,s,t}\right) \cdot \frac{1+jkr}{r^2}\cos\phi\mathrm{e}^{-\mathrm{j}kr}\Delta S, \qquad \psi \le \frac{\pi}{2}, \phi \le \frac{\pi}{2}, \quad (8)$$

where ϕ is the angle between the normal vector of the sender surface and the direction from the sender to the receiver point, ψ is the angle between the normal vector of the receiver surface and the direction from the sender to the receiver point. If ψ or ϕ is larger than $\pi/2$ the contribution is set to 0. Possible absorption at the surfaces can be accounted for by a scaling of the corresponding contribution in equation (8) with $\sqrt{1-\alpha_s}$ where α_s is the absorption coefficient of the sender surface with index s. Regarding the number of iterations needed (step 3), no general rule can be given. The order of reflections that has to be considered depends strongly on the geometry and possible absorption on the surfaces.

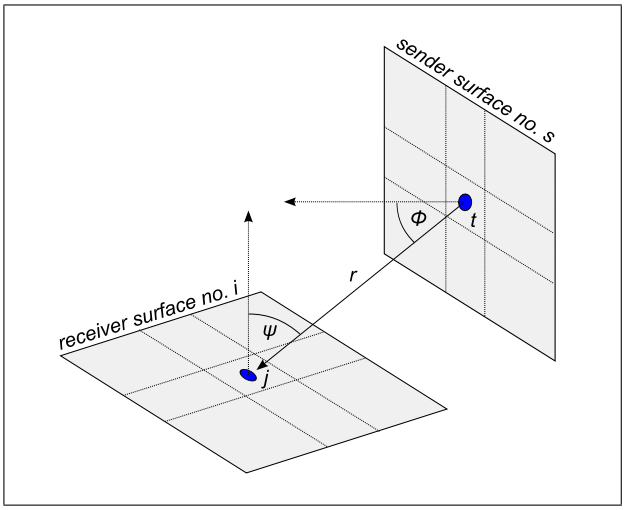

Figure 2. Situation for the iterative updating process of cell j on surface i. The geometry is shown for the contribution of cell t on surface s.

4. Model for incoherent reflections

4.1. Theoretical considerations

The physical concepts behind the model for incoherent reflections are Lambert's law and the fundamental principle of energy conservation. The sound power emitted by a sender and received by a reflecting surface is given by the product of surface area and normal component of sound intensity. It is assumed that near field effects can be ignored which means that sound pressure and velocity are in phase and their amplitude ratio equals ρc. The sound intensity vector points in the same direction as sound velocity. This direction depends only on the last sender position. For that reason no *memory* is needed that stores the history of the geometry of the sound path. The normal component of incoming sound intensity $\mathrm{d}I$ on a surface element is given by

$$\mathrm{d}I = \frac{W}{4\pi r_1^2}\cos\phi, \quad (9)$$

where W is the sound power of the sender, r_1 is the distance from the sender to the surface element, ϕ is the angle between the direction from the surface element to the sender and the normal vector of the surface. The sound power $\mathrm{d}W$ received by a surface element of area $\mathrm{d}S$ amounts to $\mathrm{d}I \cdot \mathrm{d}S$. It is assumed that dW is reflected

according to Lambert's law. In 1 m distance the reflected intensity $\mathrm{d}I(1\mathrm{m}, \psi)$ in direction ψ can be written as

$$\mathrm{d}I(1\mathrm{m}, \psi) = I_0 \cos\psi. \tag{10}$$

The constant I_0 in equation (10) has to be adjusted in such a way that the integral over the surface of a half sphere S (to represent all directions) equals the received sound power $\mathrm{d}W$.

$$\begin{aligned} \mathrm{d}W &= \int_S \mathrm{d}I(1\mathrm{m}, \psi) = \int_0^{\pi/2} I_0 \cos\psi 2\pi \sin\psi \,\mathrm{d}\psi \\ &= I_0 2\pi \frac{\sin^2\psi}{2}\Big|_0^{\pi/2} = I_0\pi. \end{aligned} \tag{11}$$

Finally, the intensity at a receiver point at distance r_2 with angle ψ to the surface normal vector stemming from $\mathrm{d}S$ is given by

$$\mathrm{d}I(r_2, \psi) = \frac{\mathrm{d}W}{\pi} \cos\psi \frac{1}{r_2^2}. \tag{12}$$

4.2. Formulation of the algorithm

The normal component of the intensity on the surface elements is used as sound field variable.

Step 1:
The surfaces S_i are divided into subareas $S_{i,j}$ of size ΔS (Fig. 1). The initial intensity is set to 0 for all surface points,

$$I_{0,i,j} = 0 \tag{13}$$

Step 2:
The first estimate of the intensity distribution $I_{1,i,j}$ on the surfaces S_i is found by calculating the propagation from the source to the receiving surfaces

$$I_{1,i,j} = \frac{W}{4\pi r^2} \cos\psi, \qquad \psi \le \frac{\pi}{2} \tag{14}$$

where W is the sound power emitted by the point source, r is the distance to the source, ψ stands for the angle between the direction from the surface point to the source and the normal vector of the surface. For $\psi > \frac{\pi}{2}$ the intensity I is set to 0.

Step 3:
The n-th estimate of the intensity distribution $I_{n,i,j}$ is found by adding the contributions of the last changes at the surface points (see Figure 2):

$$\begin{aligned} I_{n,i,j} &= I_{n-1,i,j} + \frac{1}{\pi} \sum_s \sum_t (I_{n-1,s,t} - I_{n-2,s,t}) \\ &\quad \cdot \frac{1}{r^2} \cos\phi \cos\psi \Delta S \qquad \psi \le \frac{\pi}{2}, \phi \le \frac{\pi}{2}, \end{aligned} \tag{15}$$

where ϕ is the angle between the direction from the sender surface point to the receiver surface point and the sender surface normal vector. For $\psi > \frac{\pi}{2}$ or $\phi > \frac{\pi}{2}$ the contribution I is set to 0.

Again possible absorption at the reflecting surfaces can be accounted for by a scaling of the corresponding contribution in equation (15) with $(1 - \alpha_s)$ where α_s is the absorption coefficient of the sender surface with index s.

Step 4:
Finally the intensities found according to equation (15) are converted into sound pressure values with

$$I\rho c = p'^2, \tag{16}$$

where p' is the sound pressure under free field conditions. If the façade surfaces are acoustically hard, sound pressure doubles on the surfaces. In this case one gets

$$p = 2\sqrt{I\rho c} \qquad \text{resp.} \qquad p^2 = 4I\rho c. \tag{17}$$

5. Discretization

The grid cell size for the discretization is of highest importance regarding the calculation effort. A bisection of the grid cell width increases the number of grid points by a factor of 4. As the propagation has to be evaluated from all grid points to all grid points, the calculation effort is of order n^2 where n is the number of grid points. All in all the resulting effort increases by a factor 16 corresponding to the fourth power of the grid cell width.

For the incoherent model the discretization is not very crucial, a relative coarse grid with a cell size in the order of 1 m is possible. The coherent model on the other hand reacts more sensitive to the discretization. A sufficient resolution is necessary for proper mapping of the pressure distribution. If the discretization is not fine enough, very high sound pressure values usually occur. This is a consequence of the fact that the contributions of the reflecting area cancel each other due to destructive interference. A too coarse discretization is unable to model this process properly.

The problem of required dicretization can be investigated having in mind the concept of Fresnel zones. Fresnel zones denote regions that deliver sound pressure to a receiver point with phase shifts within an interval of 180 degrees. These zone areas have to be represented with sufficient accuracy by the points of the discretization grid. The worst case is thus given for smallest Fresnel zones which corresponds to the situation of normal sound incidence and small source and receiver distances.

Here the maximum allowable grid cell size is determined numerically with the algorithm of the coherent model introduced above. To do so, a source and receiver point were assumed at the same location in distance d from a reflecting surface. The sound pressure for a first order reflection was then calculated for variable frequency f, varying distance d and varying grid cell size $\Delta x = \Delta y$. Figure 3 shows an exemplary calculation result for a reflector area of 10 by 10 meters. Depending on frequency, there is a limiting value of the grid size above which sound pressure escalates.

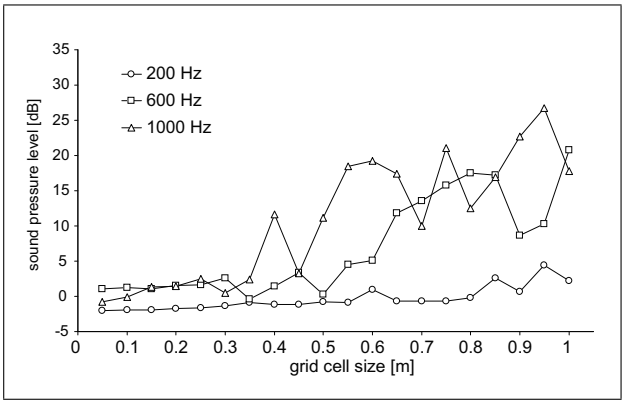

Figure 3. Influence of the grid cell size on relative sound pressure for a first order reflection. The reference 0 dB corresponds to the theoretically expected receiver level for an infinitely extended reflector. Three curves are shown for frequencies 200, 600 and 1000 Hz. The distance d of source/receiver to the reflecting surface was set to 20 m.

Table I. Maximum grid cell size $\Delta x_{\max}, \Delta y_{\max}$ as a function of frequency used in the model for coherent reflections.

Frequency [Hz]	200	400	600	800	1000
Cell size [m]	0.45	0.32	0.26	0.22	0.20

From a great number of numerical evaluations the maximum allowable grid cell size $\Delta x, \Delta y$ was found according to

$$\Delta x_{\max} = \Delta y_{\max} \approx 0.11\sqrt{d\lambda}, \tag{18}$$

where d is the distance to the reflector, λ is the wavelength. Equation (18) has strong similarity with the radius r_1 of the first Fresnel zone for large distances d,

$$r_1 = \sqrt{d\frac{\lambda}{2} + \frac{\lambda^2}{16}} \approx \sqrt{d\frac{\lambda}{2}} \quad \text{for} \quad d \gg \frac{\lambda}{8}. \tag{19}$$

From a comparison of equation (18) and (19 follows) that $\Delta x_{\max} = \Delta y_{\max}$ is about 16% of the radius of the first Fresnel zone.

In practice, a reasonable assumption for distances between reflectors in an urban environment is $d = 10$ m. From that follows the maximum grid cell size according to Table I.

6. Validation of the model for coherent reflections

6.1. General assumptions

For the validation of the coherent reflections model, comparisons with physical scale model experiments and numerical simulations with a FDTD (Finite Difference Time Domain) model were performed. The calculations were done for discrete frequencies of 250 Hz, 500 Hz and 1 kHz. The discretization of the façade surfaces was set to $\Delta x = \Delta y = 0.2$ m for all frequencies. The pressure at a distinct receiver position was calculated as average value over a circular area with radius 1.0 m. By this process the sensitivity to local interference was reduced, comparable to an averaging by integration over one octave band. All receiver levels shown below are understood relative to the level produced by the source at a distance of 1 m.

Figure 4. Source used for scale model experiments. The opening for sound radiation has a diameter of 2 mm and is located at the bottom end of the black cone.

6.2. Scale model experiments

The physical model experiments used a scale of 1:16. As a source a piezo tweeter mounted in a small cavity was used. The cavity was connected to a cone with a small opening of 2 mm for sound radiation (Figure 4). This configuration ensures an omnidirectional radiation characteristic. The cavity leads to a considerable broadening of the impulse response of the source. However, as the system under consideration can be regarded linear this results solely in a convolution of the wanted system impulse response with the impulse response of the source. The frequency range of the source extends from 3 to 40 kHz which translates into a span of 190 Hz to 2.5 kHz in real live scale. This range allows for an evaluation of the 250, 500 Hz, 1 kHz and 2 kHz octaves. Sound pressure was captured by a 1/4" B&K microphone type 4135 and fed to a MLSSA correlation measurement system. In each octave band the extra air absorption for the model frequencies was estimated and compensated. An assumed contribution at time t_0 in the impulse response travels the distance $s_0 = c \cdot t_0$ and is therefore attenuated by air absorption according to $0.001 \cdot \alpha c t_0$ [dB] where α is the air damping constant in dB/km for the corresponding frequency band and the encountered temperature and humidity and c is the speed of sound. Consequently the measured and squared impulse

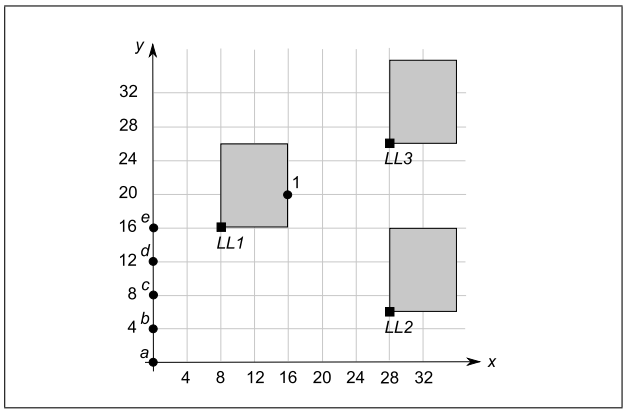

Figure 5. Definition of the geometry of situation A, consisting of five source positions *a* to *e*, three buildings with their lower left corner $LL1$ to $LL3$ and the receiver point 1. The labeling of the axis is in meters in full scale dimensions.

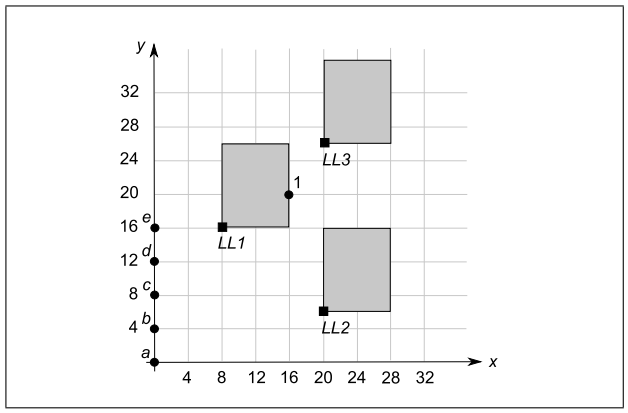

Figure 6. Definition of the geometry of situation B, consisting of five source positions *a* to *e*, three buildings with their lower left corner $LL1$ to $LL3$ and the receiver point 1.

Table II. Measured (M) sound pressure levels [dB] at the receiver position for the five source positions *a* to *e* in the three octave bands 250, 500 and 1000 Hz. The columns (C−M) give the level differences between calculated and measured values.

	M:250	C−M	M:500	C−M	M:1000	C−M
a	-27.1	1.0	-25.4	-0.2	-24.9	0.3
b	-29.5	1.1	-29.2	0.5	-27.4	0.2
c	-32.7	0.7	-33.4	-0.4	-34.4	-0.1
d	-33.9	-1.9	-36.8	-2.3	-39.8	-1.7
e	-39.8	0.7	-41.5	-1.6	-45.0	-0.9

Table III. Measured (M) sound pressure levels [dB] at the receiver position for the five source positions *a* to *e* in the three octave bands 250, 500 and 1000 Hz. The columns (C−M) give the level differences between calculated and measured values.

	M:250	C−M	M:500	C−M	M:1000	C−M
a	-30.6	-2.7	-33.3	-0.2	-36.2	3.1
b	-33.4	-2.3	-35.6	-1.1	-39.1	0.5
c	-36.4	-1.2	-37.1	-3.2	-41.1	-1.3
d	-35.7	-5.2	-37.9	-4.8	-41.8	-3.0
e	-41.6	-1.9	-42.4	-2.6	-45.1	-1.0

response $h_n^2(t)$ in frequency band n is transformed into the corrected energy impulse response $h_n'^2(t)$ according to

$$h_n'^2(t) = h_n^2(t) 10^{(\alpha_n \cdot t/29.412)}. \quad (20)$$

The geometries investigated consisted of three cuboid buildings of full scale dimensions 10×8×9 m (length × width × height) with smooth and acoustically hard surfaces. The buildings stood on the plane $z = 0$ and had always the same orientation with the longest side pointing in the y direction. The receiver was positioned at a height of 4 m directly on the surface of one of the buildings. Compared to free field, this leads to a sound pressure doubling. For each arrangement of buildings, five identical point source locations with height $z = 0$ were investigated, delivering five sound pressure octave band spectra at the receiver point.

Case A

Figure 5 shows the geometry of situation A. A valid first order specular reflection occurs for source positions *a* and *b*. Table II lists the measured and calculated sound pressure levels.

Case B

Figure 6 shows the geometry of situation B. A valid first order specular reflection occurs for none of the source positions. Table III lists the measured and calculated sound pressure levels.

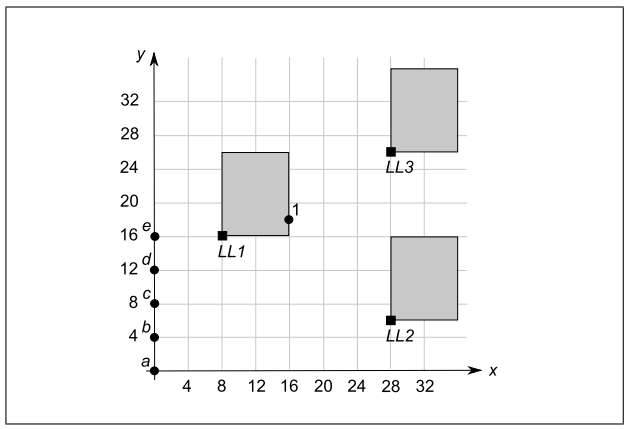

Figure 7. Definition of the geometry of situation C, consisting of five source positions *a* to *e*, three buildings with their lower left corner $LL1$ to $LL3$ and the receiver point 1.

Case C

Figure 7 shows the geometry of situation C. A valid first order specular reflection occurs for the source positions *a, b, c*. Table IV lists the measured and calculated sound pressure levels.

Case D

Figure 8 shows the geometry of situation D. A valid first order specular reflection occurs for the source positions *a, b, c, d*. Table V lists the measured and calculated sound pressure levels.

Table IV. Measured (M) sound pressure levels [dB] at the receiver position for the five source positions *a* to *e* in the three octave bands 250, 500 and 1000 Hz. The columns (C−M) give the level differences between calculated and measured values.

	M:250	C−M	M:500	C−M	M:1000	C−M
a	-24.2	0.5	-25.1	-2.2	-24.3	-1.3
b	-25.3	0.2	-24.4	-1.0	-23.8	-1.1
c	-28.2	0.2	-28.2	0.7	-26.0	0.2
d	-30.3	-1.7	-32.7	0.0	-33.8	0.8
e	-36.9	0.9	-39.1	1.1	-42.1	2.1

Table V. Measured (M) sound pressure levels [dB] at the receiver position for the five source positions *a* to *e* in the three octave bands 250, 500 and 1000 Hz. The columns (C−M) give the level differences between calculated and measured values.

	M:250	C−M	M:500	C−M	M:1000	C−M
a	-25.6	1.4	-24.2	-1.1	-25.6	-1.7
b	-24.6	0.7	-25.4	-2.8	-24.6	-1.4
c	-25.7	-0.6	-24.9	-2.4	-24.2	-2.2
d	-23.9	-0.9	-24.6	-0.1	-23.5	0.1
e	-31.3	-7.0	-32.0	-3.4	-33.0	-2.9

Table VI. With FDTD simulated (F) sound pressure levels [dB] at receiver position 1 for the five source positions *a* to *e* in the three octave bands 250, 500 and 1000 Hz. The columns (C−F) give the level differences between calculated and FDTD simulated values.

	F:250	C−F	F:500	C−F	F:1000	C-F:000
a	-24.0	0.6	-23.3	-1.7	-24.5	0.9
b	-21.7	0.4	-22.8	-1.6	-24.1	1.6
c	-20.0	0.4	-22.3	0.6	-22.8	1.2
d	-19.6	0.5	-19.3	-0.7	-21.8	1.1
e	-20.3	-0.8	-20.0	-1.3	-19.3	-0.8

6.3. Numerical simulations with FDTD

Four additional test cases were generated by calculating sound propagation in a built-up situation with a reference model based on wave theory. Here a 2D Finite Difference Time Domain (FDTD) algorithm with space discretization of 0.02 m was used [17, 18]. By applying a pressure pulse as initial condition and observing the development of the sound field in time, an impulse response can be found at any of the grid points. With the simplifying assumption that the buildings are much higher than the first Fresnel zones on the façade surfaces, the 2D results can be extended to the 3D case by weighting the pressure impulse responses with $1/\sqrt{r}$ where $r = ct$ and c is the speed of sound and t is time. After Fourier transformation, spectral information is available and can be displayed for example as octave band levels at the receiver point.

As for the scale model experiments, the geometry investigated with FDTD consisted of three cuboid buildings *K, L, M* with smooth and acoustically hard surfaces (Figure 9). Again the buildings had a height of 9 m and stood on the plane $z = 0$. The four receivers at height 4 m

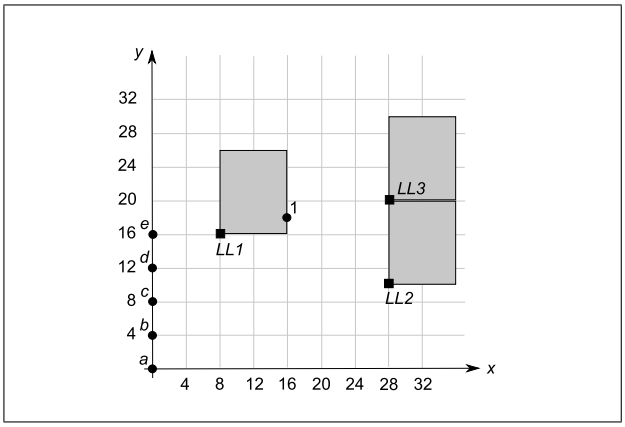

Figure 8. Definition of the geometry of situation D, consisting of five source positions *a* to *e*, three buildings with their lower left corner $LL1$ to $LL3$ and the receiver point 1.

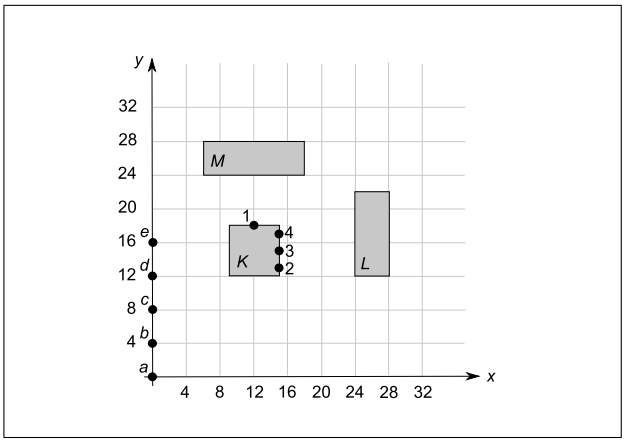

Figure 9. Geometry of the FDTD model.

were assumed flush mounted with the surface of one of the buildings (pressure doubling). For each receiver point five identical point source positions at height $z = 0$ were investigated, delivering five sound pressure octave band spectra at the receiver points.

Case E: receiver position 1

A valid first order specular reflection at receiver position 1 occurs for the source positions *a, b, c, d, e*. Furthermore there are valid higher order reflections. Table VI lists the measured and calculated sound pressure levels.

Case F: receiver position 2

A valid first order specular reflection at position 2 occurs for the source positions *d, e*.Table VII lists the measured and calculated sound pressure levels.

Case G: receiver position 3

A valid first order specular reflection at position 3 occurs for the source positions *b, c*. Source position *e* leads to a second order reflection. Table VIII lists the measured and calculated sound pressure levels.

Case H: receiver position 4

A valid first order specular reflection at position 4 occurs for the source positions *a, b*. The source positions *a, b, c* lead to a third order reflection.Table IX lists the measured and calculated sound pressure levels.

Table VII. With FDTD simulated (F) sound pressure levels [dB] at receiver position 2 for the five source positions *a* to *e* in the three octave bands 250, 500 and 1000 Hz. The columns (C−F) give the level differences between calculated and FDTD simulated values.

	F:250	C−F	F:500	C−F	F:1000	C−F
a	-30.4	-4.3	-32.6	-3.9	-36.0	7.0
b	-30.4	-0.9	-31.8	-4.2	-35.2	-2.7
c	-27.4	1.9	-29.0	-2.9	-32.0	-0.4
d	-29.5	-1.0	-30.0	0.7	-31.0	1.6
e	-24.9	-2.3	-23.5	0.9	-26.5	1.5

Table VIII. With FDTD simulated (F) sound pressure levels [dB] at receiver position 3 for the five source positions *a* to *e* in the three octave bands 250, 500 and 1000 Hz. The columns (C−F) give the level differences between calculated and FDTD simulated values.

	F:250	C−F	F:500	C−F	F:1000	C−F
a	-31.6	1.8	-34.4	1.6	-36.4	8.6
b	-28.4	0.7	-30.0	1.1	-31.1	1.0
c	-25.9	3.2	-25.8	3.4	-25.4	2.9
d	-29.7	-2.5	-30.7	-2.4	-34.8	-1.8
e	-25.5	-2.8	-25.7	1.4	-25.6	1.5

Table IX. With FDTD simulated (F) sound pressure levels [dB] at receiver position 4 for the five source positions *a* to *e* in the three octave bands 250, 500 and 1000 Hz. The columns (C−F) give the level differences between calculated and FDTD simulated values.

	F:250	C−F	F:500	C−F	F:1000	C−F
a	-28.6	0.3	-28.4	-0.1	-29.2	2.2
b	-25.9	1.4	-23.4	-2.2	-24.5	0.4
c	-25.7	-0.4	-27.4	-1.5	-29.9	1.2
d	-29.6	-3.3	-32.8	-0.5	-34.4	-6.5
e	-27.2	-0.5	-28.6	-0.3	-29.8	1.2

Table X. Statistics of the coherent model deviations to the measurements and FDTD simulations.

	250 Hz	500 Hz	1000 Hz
average [dB]	0.6	1.0	-0.3
standard deviation [dB]	2.0	1.8	2.6

6.4. Discussion

The test cases A to H show that the sound pressure at a receiver drops off relatively slowly if the source is moved away from the region where specular reflections hit the receiver. This transition is reproduced to good accuracy with the proposed coherent model. On the other hand pure geometrical approaches such as ray tracing (assuming to create specular reflections) or mirror source models can make no statement for 'shadow zones'. Consequently these models heavily underestimate the reflected sound pressure in situations with no valid mirror source (e.g. source positions *c, d, e* in case A).

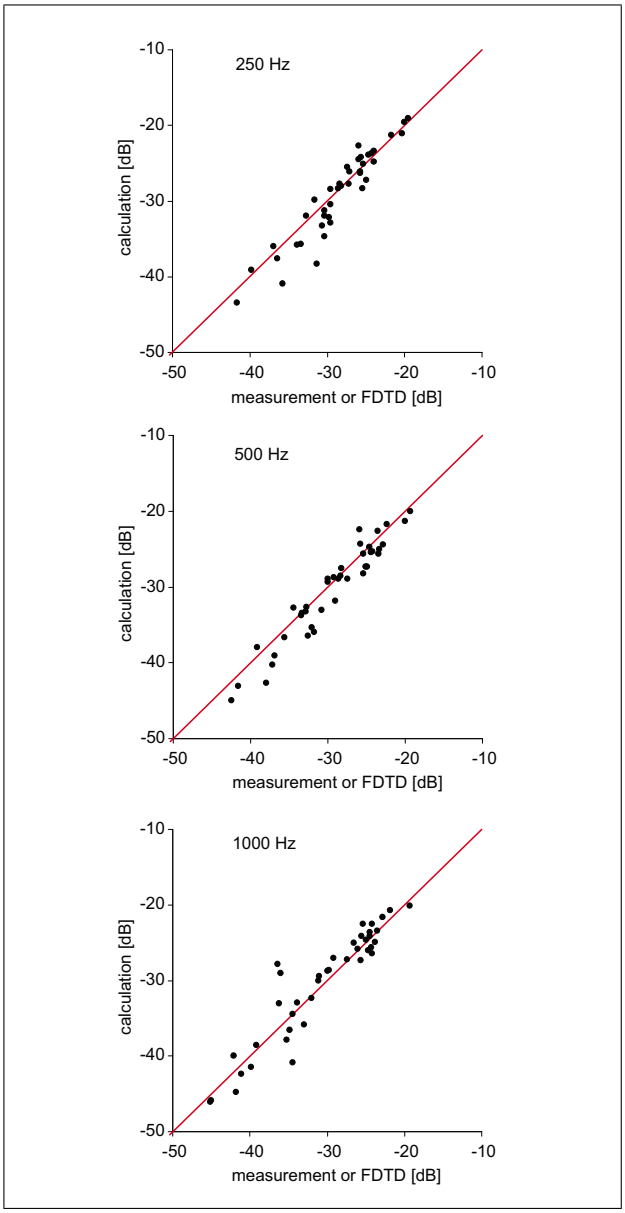

Figure 10. XY plots of the deviations between the coherent model and scale model measurements and FDTD simulations. All dB values are understood relative to a reference level in 1 m distance.

Taking into account all comparisons from above, the statistics shown in Table X is found. Figure 10 shows the corresponding XY plots. With 7.0 and 8.6 dB the largest deviations are found at 1000 Hz for the source position *a* in the test cases F and G. In both cases the reflections are weak and overestimated by the proposed model compared to the FDTD simulations. These differences are frequency dependent and occur only at 1000 Hz. This leads to the assumption that the low sound pressures found in FDTD are the consequence of an interference effect between reflected and diffracted sound.

With the exception of outliers mentioned above, there is generally a good agreement between the new model and the measurements and wave theoretical calculations respectively. The average differences are below 1 dB, the

standard deviations are somewhat larger, however, for extended sources such as roads or railway lines the error of the total sound exposure reduces significantly due to averaging over several source positions.

7. Conclusions

Two algorithms are presented to calculate diffuse and mirror like reflections in an accurate way. The scheme for diffuse or incoherent reflections is frequency independent and based on the principle of energy conservation and comparable to the radiosity method. Specular or coherent reflections are handled by an iterative solution of the Kirchhoff-Helmholtz integral. Compared to the mirror source concept, the method proposed here shows continuous behavior as there is no need for YES/NO decisions in connection with shadow zones and the validity of mirror sources. Furthermore, form and size of the reflecting surfaces and their influence on the reflection strength are considered.

From a formal point of view both algorithms presented - for diffuse and coherent reflections - are identical. However, as the two algorithms calculate different sound field variables, they can not be mixed. After the selection of a frequency it has to be decided whether the coherent or the incoherent model has to be applied. For typically structured façades, it is appropriate to use the coherent model in the lower frequency range. For wave lengths in the same order of magnitude as the structure depths, the diffuse model is applied. As an indicatory value for typical façades the transition frequency can be set to 600 Hz. An advantage as well as a difficulty of the coherent model is the fact that a single frequency sound pressure distribution on the boundaries shows high local variability due to interference effects. While evaluating a third-octave or octave band level at a certain receiver position this interference effect would be reduced significantly. This is because the interference pattern is strongly dependent on frequency. For computational reasons it is preferable to use as less frequencies as possible. On the other hand there is already information at no cost about the local variation. Thus it suggests itself to perform an averaging over space and not over frequency. The resulting receiver levels have then to be understood as representative for a small region around the receiver point itself. A circular area of 1 m radius has proven to be appropriate.

Acknowledgement

This work was financed by the Swiss Federal Office for the Environment as part of the development of the new Swiss railway noise model sonRAIL.

References

[1] J. Picaut, L. Simon: A scale model experiment for the study of sound propagation in urban areas. Applied Acoustics **62** (2001) 327–340.

[2] M. Hornikx, J. Forssen: A scale model study of parallel urban canyons. Acta Acustica united with Acustica **94** (2008) 265–281.

[3] M. R. Ismail, D. J. Oldham: Computer modelling of urban noise propagation. Building Acoustics **10** (2003) 221–253.

[4] J. Kang: Sound propagation in street canyons: Comparison between diffusely and geometrically reflecting boundaries. J. Acoust. Soc. Am. **107** (2000) 1394–1404.

[5] J. Kang: Urban sound environment. Spon Press, 2006.

[6] R. Makarewicz, I. Krasnowska: Traffic noise attenuation in an urban area in terms of A-weighted sound exposure level. Applied Acoustics **37** (1991) 65–74.

[7] K. Heutschi: A simple method to evaluate the increase of traffic noise emission level due to buildings, for a long straight street. Applied Acoustics **44** (1995) 259–274.

[8] K. P. Lee, H. G. Davies: Nomogram for estimating noise propagation in urban areas. J. Acoust. Soc. Am. **57** (1975) 1477–1480.

[9] K. K. Iu, K. M. Li: The propagation of sound in narrow street canyons. J. Acoust. Soc. Am. **112** (2002) 537–550.

[10] H. G. Davies: Multiple-reflection diffuse-scattering model for noise propagation in streets. J. Acoust. Soc. Am. **64** (1978) 517–521.

[11] J. Picaut, L. Simon, J. Hardy: Sound field modeling in streets with a diffusion equation. J. Acoust. Soc. Am. **106** (1999) 2638–2645.

[12] J. Picaut: Numerical modeling of urban sound fields by a diffusion process. Applied Acoustics **63** (2002) 965–991.

[13] J. Kang: Numerical modelling of the sound fields in urban streets with diffusely reflecting boundaries. J. Sound and Vib. **258** (2002) 793–813.

[14] K. Heutschi: Parameter study of the insertion loss reduction in case of a building facade parallel to a noise barrier. Acta Acustica united with Acustica **89** (2003) 908–912.

[15] M. Oegren, W. Kropp: Road traffic noise propagation between two dimensional city canyons using an equivalent sources approach. Acta Acustica united with Acustica **90** (2004) 293–300.

[16] T. Van Renterghem, E. Salomons, D. Botteldooren: Parameter study of sound propagation between city canyons with a coupled FDTD-PE model. Applied Acoustics **67** (2006) 487–510.

[17] D. Botteldooren: Finite-difference time-domain simulation of low-frequency room acoustic problems. J. Acoust. Soc. Am. **98** (1995) 3302–3308.

[18] K. Heutschi, M. Horvath, J. Hofmann: Simulation of ground impedance in finite difference time domain calculation of outdoor sound propagation. Acta Acustica united with Acustica **91** (2005) 35–40.